




SHLD2 promotes class switch recombination by preventing inactivating deletions within the *Igh* locus

Alexanda K Ling¹, Meagan Munro², Natasha Chaudhary², Conglei Li¹, Maribel Berru¹, Brendan Wu¹ , Daniel Durocher^{2,3}  & Alberto Martin^{1,*} 

Abstract

The newly identified shieldin complex, composed of SHLD1, SHLD2, SHLD3, and REV7, lies downstream of 53BP1 and acts to inhibit DNA resection and promote NHEJ. Here, we show that *Shld2*^{-/-} mice have defective class switch recombination (CSR) and that loss of SHLD2 can suppress the embryonic lethality of a *Brca1*⁴¹¹ mutation, highlighting its role as a key effector of 53BP1. Lymphocyte development and RAG1/2-mediated recombination were unaffected by SHLD2 deficiency. Interestingly, a significant fraction of *Shld2*^{-/-} primary B-cells and 53BP1- and shieldin-deficient CH12F3-2 B-cells permanently lose expression of immunoglobulin upon induction of CSR; this population of Ig-negative cells is also seen in other NHEJ-deficient cells and to a much lesser extent in WT cells. This loss of Ig is due to recombination coupled with overactive resection and loss of coding exons in the downstream acceptor constant region. Collectively, these data show that SHLD2 is the key effector of 53BP1 and critical for CSR *in vivo* by suppressing large deletions within the *Igh* locus.

Keywords B cell; BRCA1; class switch recombination; shieldin; *Shld2*^{-/-} mouse

Subject Categories DNA Replication, Recombination & Repair; Immunology

DOI 10.15252/embr.201949823 | Received 5 December 2019 | Revised 19 May 2020 | Accepted 25 May 2020 | Published online 17 June 2020

EMBO Reports (2020) 21: e49823

Introduction

Across multiple phyla, adaptive immunity requires programmed DNA damage and concomitant repair to generate antigen receptor diversity and fine-tune the immune response. These phenomena are also particularly well suited for studying the various DNA repair pathways responsible for maintaining genome integrity. In particular, the humoral response mediated by B-cells requires the non-homologous end-joining (NHEJ) repair pathway for V(D)J

recombination of the antigen-binding immunoglobulin (Ig) variable region, as well as class switch recombination (CSR) of the Ig constant regions (Kenter, 2005). Activation-induced cytidine deaminase (AID) plays a central role in humoral immunity by inducing somatic hypermutation (SHM) and CSR that function to increase the antibody affinity and alter the antibody isotype, respectively (Muramatsu *et al*, 2000). AID accomplishes these processes by deaminating dC to produce dU within the immunoglobulin DNA encoding the variable region and the non-coding switch regions (Martin *et al*, 2002; Petersen-Mahrt *et al*, 2002; Bransteitter *et al*, 2003). At this point, both processes diverge: In the context of SHM, damage produced by AID at the variable region is engaged by base excision repair and mismatch repair pathways leading to small mutations that may potentially increase the affinity of the antibody to antigen (Cascalho *et al*, 1998; Wiesendanger *et al*, 2000; Di Noia & Neuberger, 2002; Martin *et al*, 2003; Rada *et al*, 2004; Wilson *et al*, 2005). By contrast in CSR, damage produced by AID at the switch μ (S μ) and downstream switch regions (S γ , S ϵ , and S α) is engaged by the same DNA repair pathways, with the distinction that these lesions are converted to double-stranded DNA breaks (DSBs), followed by synapsis and ligation of distant ends through NHEJ or the poorly defined alternative end joining (Pan *et al*, 2002; Kenter, 2005; Masani *et al*, 2016). The process of CSR allows for the expression of a novel downstream Ig constant region, with differing effector functions, with the pre-existing variable region.

The joining reaction during CSR requires the NHEJ pathway. One member, 53BP1, plays a key role in CSR (Manis *et al*, 2004) by inhibiting DNA end resection (Bothmer *et al*, 2010; Bunting *et al*, 2010), thereby shuttling the repair of DSBs toward NHEJ instead of the homologous recombination pathway. Downstream of 53BP1 lies RIF1 that further facilitates DNA end protection and is necessary for CSR (Chapman *et al*, 2013; Di Virgilio *et al*, 2013; Escribano-Diaz *et al*, 2013; Zimmermann *et al*, 2013). The recently identified shieldin complex, that lies immediately downstream of the 53BP1-RIF1 axis, is necessary for CSR, NHEJ, and telomere protection (Dev *et al*, 2018; Findlay *et al*, 2018; Ghezraoui *et al*, 2018; Gupta *et al*, 2018; Noordermeer *et al*, 2018; Tomida *et al*, 2018). Shieldin is

¹ Department of Immunology, University of Toronto, Toronto, ON, Canada

² Lunenfeld-Tanenbaum Research Institute, Mount Sinai Hospital, Toronto, ON, Canada

³ Department of Molecular Genetics, University of Toronto, Toronto, ON, Canada

*Corresponding author. Tel: +1 416 978 4230; E-mail: alberto.martin@utoronto.ca

composed of REV7, SHLD1, SHLD2, and SHLD3. SHLD2 has three OB-fold domains that bind to single-stranded DNA (Noordermeer *et al*, 2018; Setiaputra & Durocher, 2019), much like RPA1 and POT1 proteins, and appears to be the factor proximally responsible for the end protection role ascribed to the 53BP1 pathway (Dev *et al*, 2018; Findlay *et al*, 2018; Gupta *et al*, 2018; Noordermeer *et al*, 2018; Tomida *et al*, 2018). Some shieldin components have been demonstrated to promote CSR in B-cell lines (Gupta *et al*, 2018; Noordermeer *et al*, 2018), and 53BP1/RIF1/REV7-deficient mice have also been observed to have profoundly impaired CSR (Manis *et al*, 2004; Chapman *et al*, 2013; Di Virgilio *et al*, 2013; Ghezraoui *et al*, 2018). By contrast, the importance of SHLD1, SHLD2, and SHLD3 on CSR in mice has not been tested. In this report, we show that SHLD2 deficiency impairs CSR in mice but has no impact on early B-cell development and V(D)J recombination. We further show that *Shld2*^{-/-} primary B-cells, as well as 53BP1-, shieldin-, and other NHEJ-deficient CH12F3-2 B-cells (hereafter referred to as CH12 cells), exhibit a significant population with low-to-no expression of Ig upon induction of CSR. This effect is permanent as cells do not recover Ig expression. Our analysis shows that a large proportion of these Ig^{lo} CH12 cells have undergone CSR to IgA, however with major deletions of the *Ighm* and *Igha* loci that lead to loss of C α constant region exons. These data suggest that 53BP1 or shieldin deficiency does not lead to reduced recombination at the DNA level *per se*, but rather to a relative increase in non-productive CSR that inactivates the *Igh* locus. These results also support a role of the shieldin complex in preventing resection of DNA.

Results

Lymphocyte development and B-cell populations largely unaffected by *Shld2* deficiency

Shld2 knockout mice (*Shld2*^{em_{del}/em_{del}}, referred hereafter as *Shld2*^{-/-}) were generated by microinjection of Cas9 ribonucleoprotein complexes targeting exon 4 in the C57BL/6 background, and a founder mouse with a large out-of-frame deletion (248 bp) was generated (Fig 1A). Histopathology examination of various organs and tissues reported no significant pathologies in the *Shld2*^{-/-} mice relative to controls (see Materials and Methods).

One of the most remarkable genetic interaction observed among DNA repair-coding genes is the ability of 53BP1 mutations to suppress the embryonic lethality and cell lethality associated with *BRCA1* loss-of-function alleles (Cao *et al*, 2009; Bouwman *et al*, 2010; Bunting *et al*, 2010). There is currently some debate as to which effector of 53BP1 is responsible to enforce lethality in *BRCA1* mutants since the loss PTIP-interacting 53BP1-S25 residue in mice results in viable *Brca1*^{A11/A11} animals suggesting that PTIP is a critical mediator of the embryonic lethality of *BRCA1*-deficient animals. However, *Brca1*^{A11/A11}; *53bp1*^{S25A/S25A} mice display phenotypes such as premature aging, and mouse embryo fibroblasts derived from these mice remain profoundly HR-deficient due to the presence of the RIF1-shieldin axis (Callen *et al*, 2019). To test the impact of shieldin depletion on the viability of the *Brca1*^{A11} allele (exon 11 deleted), we combined the *Shld2*-null allele with the *Brca1*^{A11} mutation by *Shld2*^{-/+}; *Brca1*^{A11/+} x *Shld2*^{-/+}; *Brca1*^{A11/+} intercrosses. We monitored the genotype of 96 live births and found that

introduction of the *Shld2* mutation suppressed the embryonic lethality of the *Brca1*^{A11} allele (Xu *et al*, 2001) (Table 1; $\chi^2 = 33.208$, $P = 5.649 \times 10^{-5}$). At the time of submission, all double-mutant mice were alive and appeared normal, with the oldest mouse being 27.5 weeks old. These results indicate that SHLD2 is a key effector of 53BP1 with respect to the lethality of BRCA1 loss.

In *Shld2*^{-/-} mice, there was no apparent block in B- and T-cell development in the bone marrow and thymus, respectively, particularly at the Hardy fraction C or DN3 populations corresponding to the pre-BCR and pre-TCR selection stages (Figs 1B and C, and EV1A and D). Moreover, marginal zone and follicular B-cells in the spleen, as well as B1 cells in the peritoneal cavity, were unaffected by SHLD2 deficiency (Figs 1D and E, and EV1B and C). This apparent lack of a defect in lymphocyte development suggests that V(D)J recombination mediated by the RAG1/2 recombinase is unaffected by SHLD2 deficiency. To test this notion, we transduced A70.2 INV-4 cell line with CRISPR lentivirus targeting the *53bp1*, *Shld1*, *Shld2*, *Shld3*, and *Lig4* genes. In this cell line, imatinib-induced RAG-mediated recombination of a genomically integrated artificial substrate results in GFP expression (Bredemeyer *et al*, 2006). In the bulk-edited A70.2 cells, despite similar indel penetrance using the various CRISPR constructs and low baseline frequency of GFP expression (Fig EV1E and F), the only defect in GFP expression was in cells transduced with *Lig4*-targeting sgRNA (Fig 1F). Hence, SHLD2 deficiency does not impact V(D)J recombination, consistent with what was observed in the *Mb1*^{cre/+} *Rev7*^{fl/fl} mice (Ghezraoui *et al*, 2018).

SHLD2 is necessary for class switch recombination

To determine whether SHLD2 functions in CSR *in vivo*, we first examined the steady-state levels of serum Ig isotypes. We found that the levels of IgM in the serum of unimmunized *Shld2*^{-/-} mice were normal, but IgG2b and IgG3 isotypes had reduced concentrations relative to wild type (Fig 2A). Interestingly, IgA levels seemed to be elevated in *Shld2*^{-/-} animals, perhaps pointing to a reduced dependence of IgA CSR on NHEJ, as previously reported (Li *et al*, 2018). To further test the role of SHLD2 in CSR, we purified splenic B-cells and induced them to switch to various isotypes using different stimulation cocktails. We found that *ex vivo* CSR to all tested Ig isotypes shows a clear impairment of *Shld2*^{-/-} B-cells relative to WT (Figs 2B and EV2A), and this impairment was not due to a decrease in AID protein or sterile transcript expression (Fig EV2B and C). In addition, using an experimental system in which class switch is mediated by Cas9 (Ling *et al*, 2018), we found that neither 53BP1 nor SHLD2 deficiency affected this pseudo-CSR (Fig EV2D). This finding is similar to previous results involving 53BP1 deficiency and I-SceI-mediated CSR (Bothmer *et al*, 2010), pointing to a unique relationship between 53BP1/shieldin function and AID-mediated DNA damage.

To examine the effect of SHLD2 on antigen-specific CSR, mice were immunized with 4-Hydroxy-3-nitrophenylacetyl Chicken Gamma Globulin (NP-CGG). *Shld2*^{-/-} mice had reduced NP-specific serum of the IgG1, IgG2a, IgG2b, and IgG3 classes relative to WT, as well as a trend to increased NP-specific IgM (Fig 2C). In some cases, the NP-specific serum Ig defect in *Shld2*^{-/-} mice was intermediate between WT and *53bp1*^{-/-} animals. In addition, *Shld2*^{-/-} splenic NP-specific IgG1-secreting cells were ~7-fold reduced compared to

WT and congruent with *53bp1*^{-/-} results (Fig 2D). Moreover, there was no apparent difference in splenic germinal center B-cell frequency before or after NP-CGG immunization, suggesting that the *Shld2*^{-/-} CSR defect is on the molecular level of end joining (Fig EV3). All together, these data show a critical function of SHLD2 in CSR in mice, supporting previous findings in the CH12 B-cell line (Noordermeer et al, 2018).

Deficiency in the shieldin complex and other NHEJ factors exhibit a permanent Ig^{lo} population upon CSR

In carrying out the *ex vivo* CSR of WT and *Shld2*^{-/-} B-cells, we observed that *Shld2*^{-/-} B-cells stimulated with LPS and IL4 showed an increased proportion of IgM^{lo} IgG1^{lo} cells relative to WT cells at day 6 post-stimulation (Fig 3A). This phenomenon was also

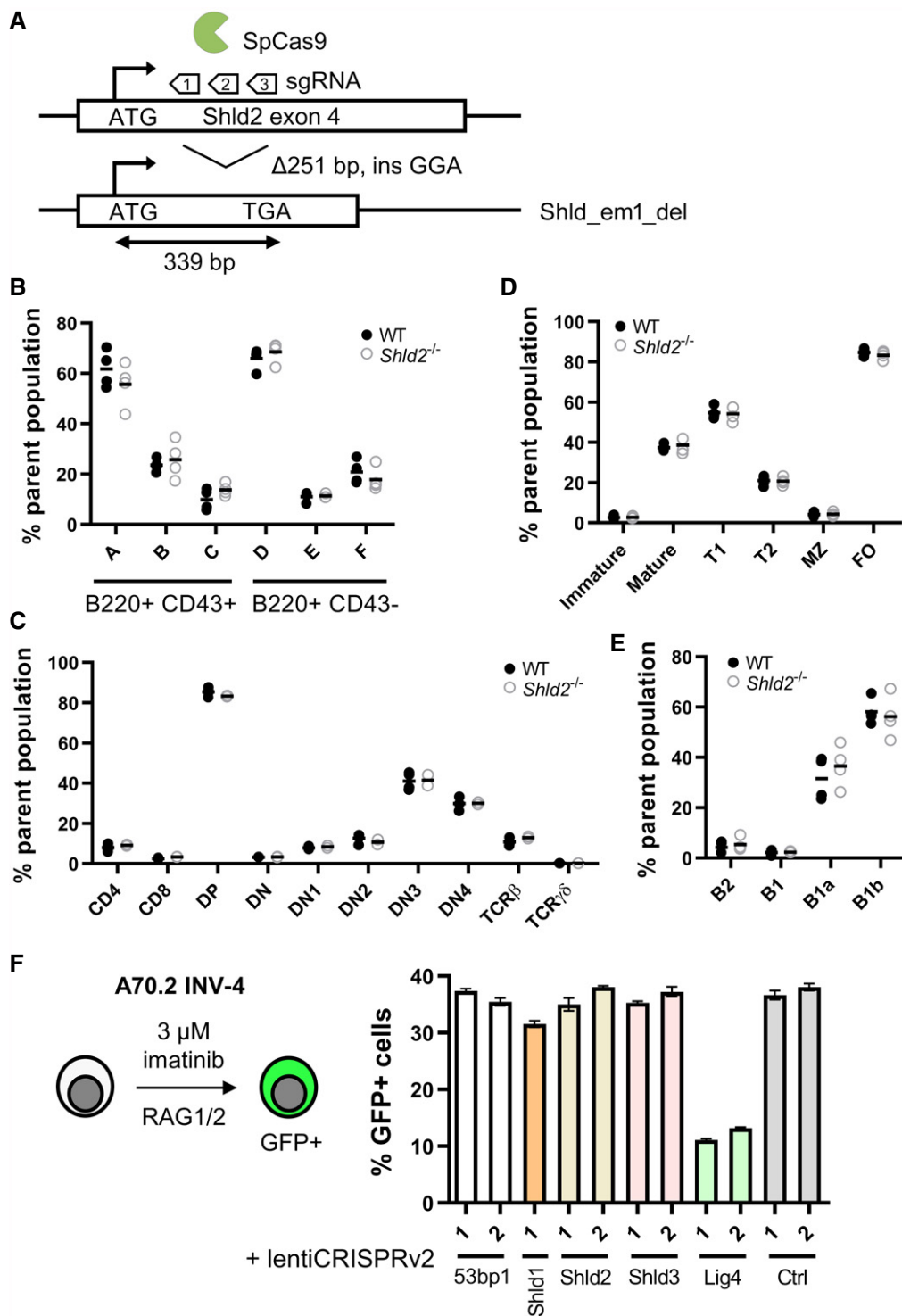


Figure 1.

Figure 1. SHLD2 does not affect lymphocyte development or V(D)J recombination.

- A Schematic of the *Shld2* exon 4 showing the 3 sgRNAs used to produce a 251 base pair deletion in one founder line that leads to a frameshift and usage of a premature stop codon.
- B Characterization of the various B-cell progenitor fractions as described by Hardy *et al* (1991) in the bone marrow of 4 wild-type and 4 *Shld2*^{-/-} littermate controls. Gating strategy for measuring these populations is shown in Fig EV1A.
- C Characterization of the indicated thymic T-cell populations in the bone marrow of 4 wild-type and 4 *Shld2*^{-/-} littermate controls. Gating strategy for measuring these populations is shown in Fig EV1D.
- D Characterization of the indicated immature and mature splenic B-cell populations in the bone marrow of 4 wild-type and 4 *Shld2*^{-/-} littermate controls. Gating strategy for measuring these populations is shown in Fig EV1B.
- E Characterization of the indicated peritoneal B-cell populations in the bone marrow of 4 wild-type and 4 *Shld2*^{-/-} littermate controls. Gating strategy for measuring these populations is shown in Fig EV1C.
- F Left panel: Schematic of the A70.2 INV-4 cell line strategy to induce RAG1/2-mediated recombination using imatinib. Right panel: A70.2 INV-4 cell lines were transduced with lentiviruses encoding the lentiCRISPRv2 expressing sgRNAs against the *53bp1*, *Shld1*, *Shld2*, *Shld3*, and *Lig4* genes. Guide RNA targeting chicken AID was used as a negative control (Ctrl). Cells were selected with puromycin and treated with 3 μM imatinib for 4 days after which GFP frequency was measured (mean ± SD of 3 biological replicates). The insertion–deletion (indel) penetrance as measured by TIDE analysis (Brinkman *et al*, 2014) of sequence for each of these sgRNA constructs is shown in Fig EV1E, and the baseline GFP frequency prior to imatinib stimulation is shown in Fig EV1F. sgRNA sequences used are shown in Table EV2.

Table 1. Genotypes of the *Shld2*^{-/-}; *Brca1*^{A11/+} × *Shld2*^{+/-}; *Brca1*^{A11/+} intercross.

Genotype	Total mice	Observed frequency	Expected frequency
<i>Shld2</i> ^{+/-} ; <i>Brca1</i> ^{+/+}	8	0.0833	0.0625
<i>Shld2</i> ^{-/-} ; <i>Brca1</i> ^{+/+}	6	0.0625	0.125
<i>Shld2</i> ^{-/-} ; <i>Brca1</i> ^{+/-}	10	0.1042	0.0625
<i>Shld2</i> ^{+/-} ; <i>Brca1</i> ^{A11/+}	12	0.1250	0.125
<i>Shld2</i> ^{-/-} ; <i>Brca1</i> ^{A11/+}	37	0.3854	0.25
<i>Shld2</i> ^{-/-} ; <i>Brca1</i> ^{A11/+}	14	0.1458	0.125
<i>Shld2</i> ^{+/-} ; <i>Brca1</i> ^{A11/A11}	0	–	0.0625
<i>Shld2</i> ^{-/-} ; <i>Brca1</i> ^{A11/A11}	0	–	0.125
<i>Shld2</i> ^{-/-} ; <i>Brca1</i> ^{A11/A11}	9	0.0938	0.0625
Total	96		

$$\chi^2 = 33.208, P = 5.649 \times 10^{-5}.$$

recapitulated in *53bp1*^{-/-}, *Shld1*^{-/-}, *Shld2*^{-/-/-}, and *Shld3*^{-/-} CH12 B-cells at 3 days after stimulating with the CIT cocktail (anti-CD40, IL4, TGFβ) that induces CSR to IgA (Fig 3B). We also found that CH12 cells deficient in other NHEJ factors such as KU70, KU80, DNA-PKcs, XLF, XRCC4, and LIG4 (but not PAXX) (Appendix Fig S1) have reduced CSR to IgA and an increased Ig^{lo} population (Fig 3B and C). The presence of this Ig^{lo} population was temporary and was reduced by 9 days post-stimulation in *ex vivo* B-cells (Fig 3A) and 7 days post-CIT stimulation in *53bp1*^{-/-}, *Shld2*^{-/-/-},

and *Shld3*^{-/-} CH12F3-2 B-cells (Fig 4A), as well as in CH12 cells deficient in *Shld1*, KU70, KU80, XLF, XRCC4, and LIG4 (Fig EV4A).

DSB formation has been shown to transiently reduce expression of a gene, a process mediated by ATM (Harding *et al*, 2015). Hence, cells deficient in NHEJ factors might have *Igh* DSBs that persist longer than in WT cells, and thus impose a longer-lasting decrease in Ig expression. To test whether this Ig^{lo} population was exhibiting a transient decrease in Ig expression or was being diluted from the population due to increased death and/or decreased proliferation, WT and mutant CH12 cells were stimulated with CIT for 3 days, and IgM⁺ IgA⁻, IgM⁻ IgA⁺, and IgM^{lo} IgA^{lo} populations from WT, *53bp1*^{-/-}, *Shld2*^{-/-/-}, and *Shld3*^{-/-} CH12 cells were sorted out and re-cultured for 5 or 12 days. Notably, all three populations from all CH12 genotypes largely maintained their Ig expression phenotype at the point of sorting (Figs 4B and EV4B). These data suggest that CSR induces a permanent reduced Ig expression in *53bp1*^{-/-} and *Shld*^{null} CH12 cells.

CSR in *53bp1*^{-/-} and *Shld2*^{-/-/-} CH12 cells leads to aberrant recombination involving deletions in the acceptor constant region

The finding that CSR induction generates a persistent Ig^{lo} population in *53bp1*^{-/-} and *Shld*^{null} CH12 cells suggests that the *Igh* locus has been inactivated. One possible explanation for this phenomenon is that *53bp1*^{-/-} and other NHEJ-deficient CH12 cells exhibited increased DNA resection during CSR, leading to loss of sequences that allow for surface expression of IgH. To test this notion, Ig^{lo} cells from WT, *53bp1*^{-/-}, and *Shld2*^{-/-/-} CH12 cells

Figure 2. SHLD2-deficient mice have defects in class switch recombination.

- A Concentration of the various indicated isotypes in the serum of 6- to 8-week-old unimmunized WT and *Shld2*^{-/-} mice. Values are mean concentration ± SD of 4 biological replicates; ***P* ≤ 0.01, unpaired two-tailed *t*-test.
- B B-cells were purified from spleens from WT and *Shld2*^{-/-} mice, and stimulated to undergo CSR to the various indicated isotypes using different stimulation cocktails (Li *et al*, 2018). Cells were then analyzed by flow cytometry for expression of the various indicated isotypes, and the percent expression of each isotype is reported. Values are mean frequency ± SD of 4 biological replicates; *****P* ≤ 0.0001, unpaired two-tailed *t*-test.
- C WT, *53bp1*^{-/-}, and *Shld2*^{-/-} mice were immunized with NP-CGG, the serum was withdrawn 2 weeks post-immunization, and serial dilutions were subjected to ELISA analysis for NP-specific antibodies of the indicated isotypes. Values are mean absorbance ± SD of 4 biological replicates.
- D WT, *53bp1*^{-/-}, and *Shld2*^{-/-} mice were immunized with NP-CGG, spleens were isolated, and anti-IgG-secreting cells were enumerated by the ELISPOT assay. Values are mean frequency ± SD of 4 biological replicates, except for *Shld2*^{-/-} (n = 3); **P* ≤ 0.05, ***P* ≤ 0.01, unpaired two-tailed *t*-test.

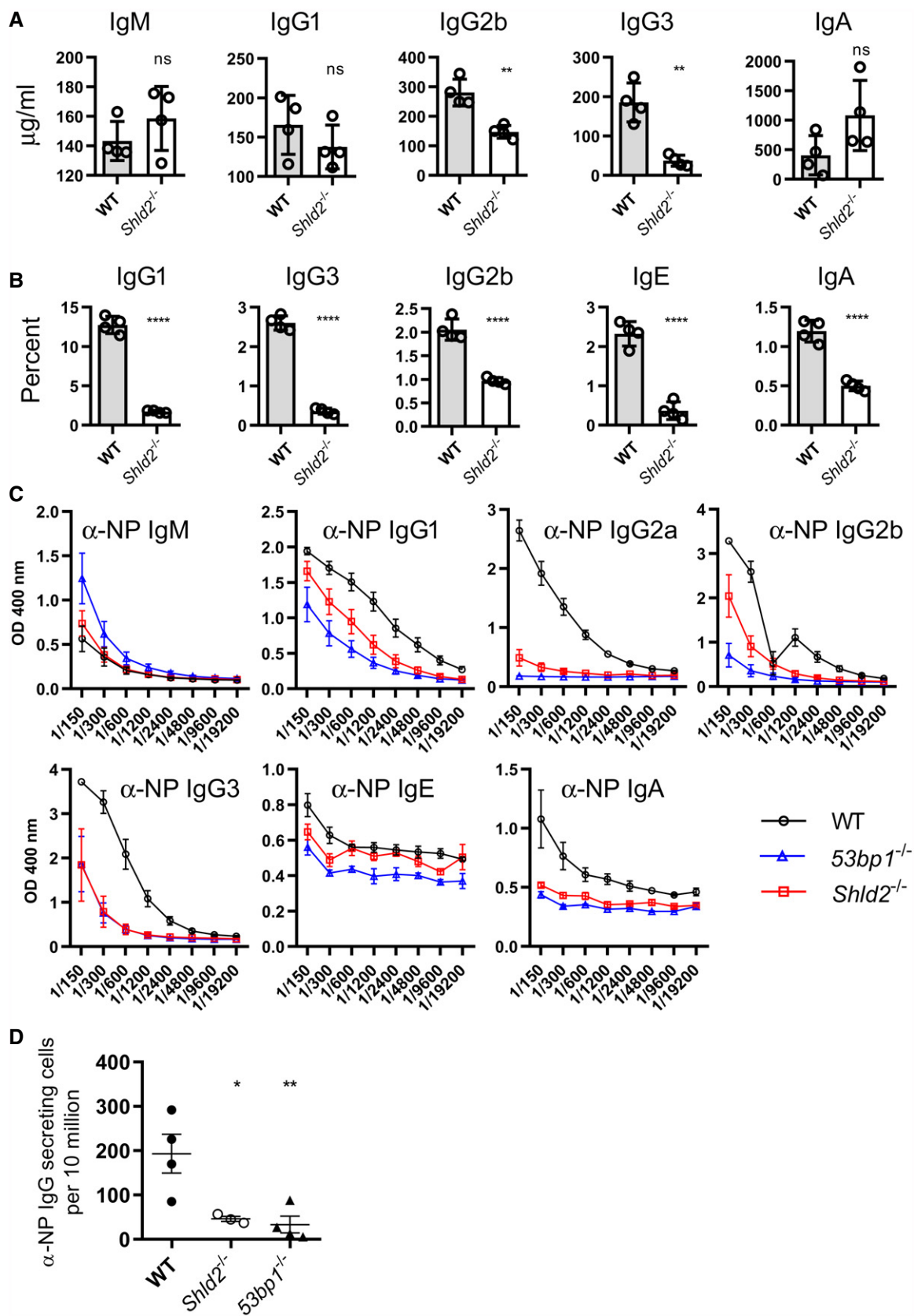


Figure 2.

were sorted, and subcloned, and expression for IgM and IgA was re-assessed by flow cytometry to confirm that Ig expression remained negative or low (Appendix Fig S2). To test whether expression of IgM or IgA was affected at the mRNA level, we used primers that amplified the entire coding region of the IgM and IgA transcript from the leader sequence to stop codon. For the WT Ig^{lo}

subclones, we found that most expressed IgA at the mRNA level; however, 50% (4/8) of tested subclones only expressed “truncated” (~0.7 kb) IgA cDNAs relative to the full-length IgA mRNA (~1.6 kb); the positive control also has a truncated IgA cDNA band likely corresponding to a mis-spliced product (Fig 5A). For the *53bp1*^{-/-} Ig^{lo} subclones, 72% (18/25) of tested subclones only

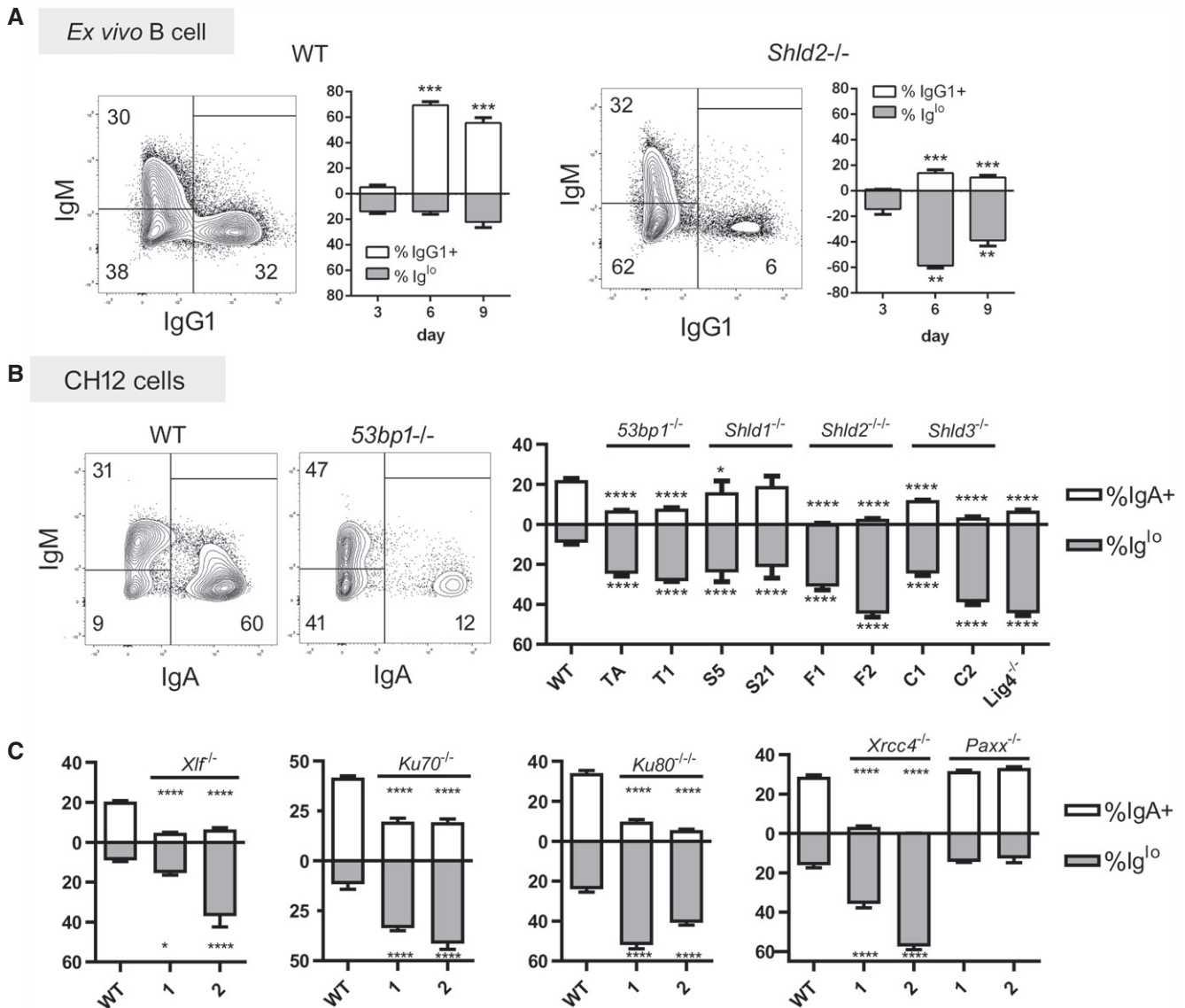


Figure 3. SHLD2-deficient B-cells and B-cells deficient in other NHEJ factors exhibit an Ig^{lo} population upon CSR induction.

A WT and *Shld2*^{-/-} B-cells were purified from spleens and stimulated with LPS + IL4 and examined for IgM and IgG1 expression 3, 6, and 9 days post-stimulation by flow cytometry. Representative plots are shown for both WT and *Shld2*^{-/-} B-cells 6 days post-stimulation. The graph plots show proportion of IgG1⁺ and Ig^{lo} cells, mean ± SD from 6 biological replicates; ***P* ≤ 0.01, ****P* ≤ 0.001, two-way ANOVA with *post hoc* Dunnett's test.

B WT CH12 cells, as well as two each of *53BP1*^{-/-}, *SHLD1*^{-/-}, *SHLD2*^{-/-}, and *SHLD3*^{-/-} deficient clones generated previously (Noordermeer et al, 2018), as well as a *LIG4*^{-/-} deficient CH12 clone, were subjected to CSR induction with the CIT cocktail and measured for both IgM and IgA expression by flow cytometry. Representative flow plots for WT and *53bp1*^{-/-} CH12 cells are shown at day 3 post-CIT stimulation. The graph plots show proportion of IgA⁺ and Ig^{lo} CH12 cells, mean ± SD from 3 biological replicates; **P* ≤ 0.05, *****P* ≤ 0.0001, two-way ANOVA with *post hoc* Dunnett's test. The letters below the x-axis represent the clone codes for the *53BP1*^{-/-}, *SHLD1*^{-/-}, *SHLD2*^{-/-}, and *SHLD3*^{-/-} deficient CH12 clones. One *LIG4*^{-/-} deficient CH12 clone was also used.

C The *Xlf*, *Ku70*, *Ku80*, *Xrcc4*, and *Paxx* genes were knocked out in CH12 cells by CRISPR, and two independent clones each were analyzed as in Fig 3B with mean ± 3 biological replicates; **P* ≤ 0.05, *****P* ≤ 0.0001, two-way ANOVA with *post hoc* Dunnett's test.

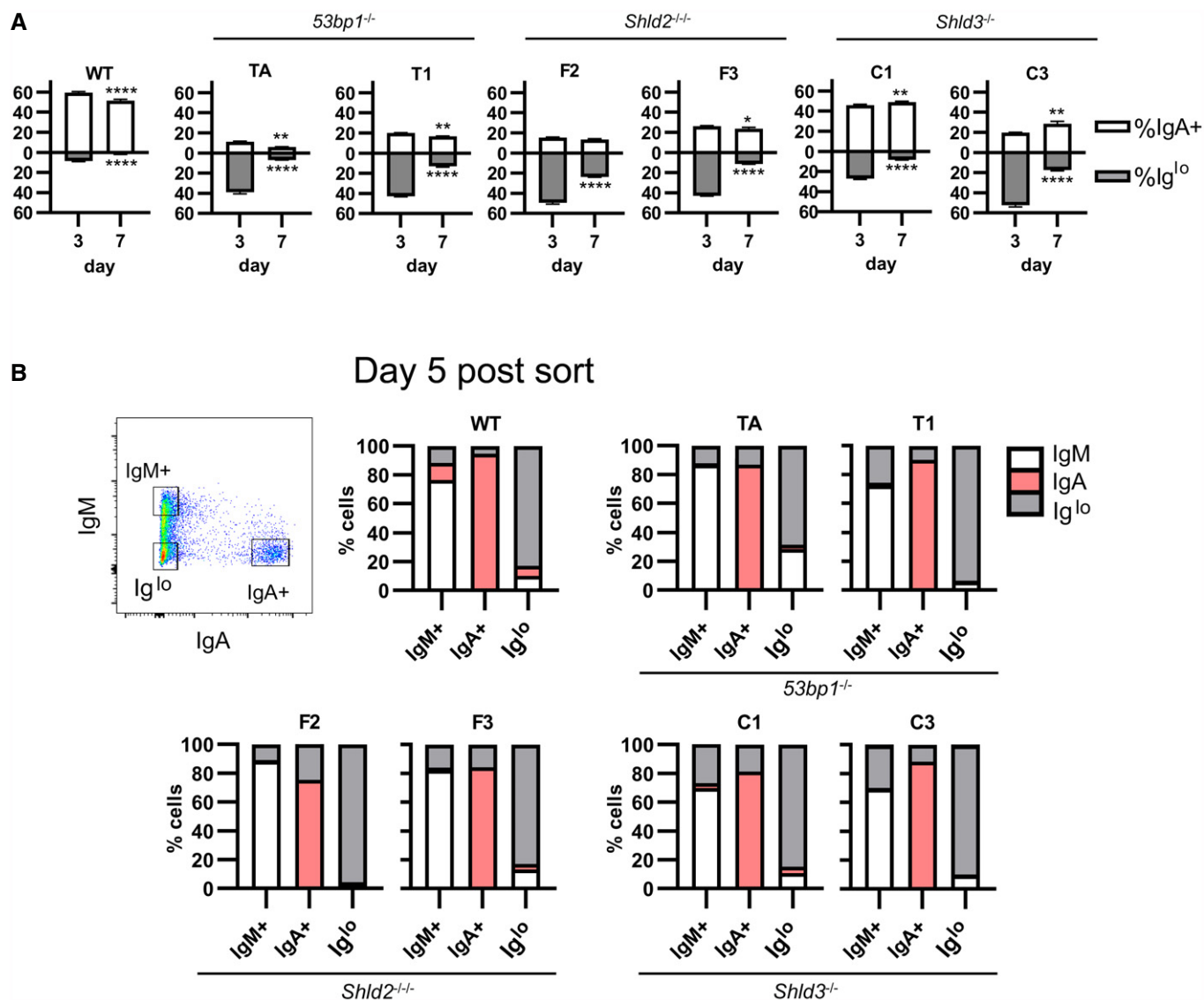


Figure 4. Reduced Ig expression in 53BP1-, SHLD2-, and SHLD3-deficient CH12 cells is permanent and dependent on CSR.

A WT and two independent clones each of *53bp1*^{-/-}, *Shld2*^{-/-}, and *Shld3*^{-/-} CH12 cells were stimulated with CIT and analyzed by flow cytometry for IgM and IgA expression. The Ig^{lo} population was reduced after 7 days in culture. Values are mean ± SD from 3 biological replicates; **P* ≤ 0.05, ***P* ≤ 0.01, *****P* ≤ 0.0001, two-way ANOVA with *post hoc* Dunnett's test.

B WT and two independent clones each of *53bp1*^{-/-}, *Shld2*^{-/-}, and *Shld3*^{-/-} CH12 clones were stimulated with CIT for 3 days. The IgM⁺, IgA⁺, and Ig^{lo} populations were sorted and reanalyzed for expression of IgM and IgA 5 days post-sort as well as 12 days post-sort (see Fig EV4B). Shown on bar graphs are sorted IgM⁺, IgA⁺, and Ig^{lo} populations (each column, 1 technical replicate) from WT and mutant CH12 clones, and the percent of cells expressing IgM, IgA, or low for both isotypes (Ig^{lo}) after 5 days of culture post-sort. A representative flow plot of *53bp1*^{-/-} CH12 3 days post-CIT treatment is shown.

expressed truncated IgA cDNAs (~0.7 or 1 kb); a small fraction of subclones expressed neither IgM or IgA cDNA, and at least one clone (D01) appeared oligoclonal by expressing both IgM and IgA transcripts (Fig 5A). Likewise, *Shld2*^{-/-} Ig^{lo} subclones also expressed truncated or no IgA transcripts, as compared with *Shld2*^{-/-} IgA⁺ subclones which expressed the full-length IgA transcript (Fig 5B).

To determine the nature of these truncated IgA cDNAs, we sequenced the IgA amplicons for select WT Ig^{lo} CH12 subclones. The analysis showed that these subclones expressed IgA mRNAs

that were variably missing exons Cα1, Cα2, and Cα3 (Fig 5C). These data suggest that many of the Ig^{lo} clones in WT, *53bp1*^{-/-}, and *Shld2*^{-/-} CH12 cells had developed deletions during CSR that either deleted or affected splicing of IgA constant region Cα exons to the variable region VDJ exon.

To confirm these deletions at the DNA level, we extracted DNA from these subclones and assayed for *Ighm* and *Igha* deletions on the assumption that most of the Ig^{lo} subclones had undergone recombination. Using a long-range PCR assay, we attempted to amplify a region between the *Ighm* Iμ exon and the *Igha* M exon

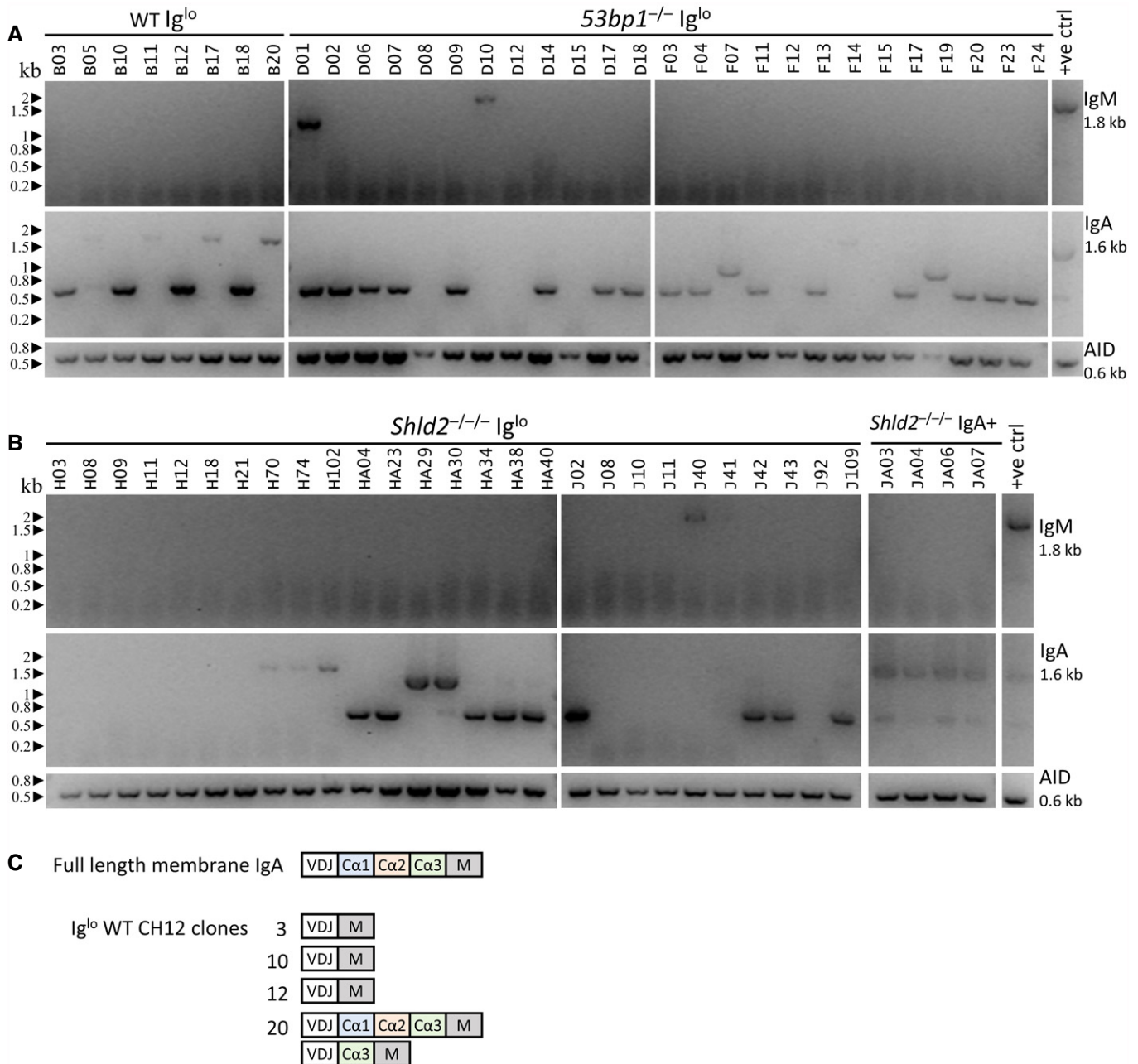


Figure 5. Loss of Ig cell-surface expression in CH12 cells is accompanied by aberrant IgA transcripts.

A mRNA expression analysis of IgM and IgA was carried out by RT-PCR for Ig^{lo} subclones from WT and two independent $53bp1^{-/-}$ CH12 (TA and T1) clones. The Ig^{lo} subclones derived from the $53bp1^{-/-}$ CH12 TA clone are listed as D01-D18, while the Ig^{lo} subclones derived from the $53bp1^{-/-}$ CH12 T1 clone are listed as F03-F24. Gels show the RT-PCR analysis for IgM cDNA (top), IgA cDNA (middle), and AID cDNA (bottom) as control. Appendix Fig S2 shows the expression of IgA and IgM by flow cytometry for each of these subclones.

B mRNA expression analysis as in A of Ig^{lo} subclones of two independent $Shld2^{-/-}$ (F2 and F3) clones and IgA^+ subclones from $Shld2^{-/-}$ clone F3. The Ig^{lo} subclones derived from the $Shld2^{-/-}$ CH12 F2 clone are listed as H03-H40, while the Ig^{lo} subclones derived from the $Shld2^{-/-}$ CH12 F3 clone are listed as J02-J109.

C Representative IgA cDNA sequence analysis from WT Ig^{lo} clones.

downstream of $Ca3$, with the maximal size of the amplicon expected to be at ~12 kb (Fig 6A). Almost all the subclones, both Ig^{lo} and IgA^+ , yielded long-range amplicons and confirmed that Ig^{lo} cells have undergone recombination (Fig 6B and C). In many cases, there was more than one amplicon from each subclone, which is likely

due to recombination of both the productive and non-productive (without the rearranged VDJ exon) *Igh* alleles; alternatively but not mutually exclusively, some of the subclones may have been or become oligoclonal at the point of or after subcloning. Moreover, many of the amplicons from $53bp1^{-/-}$ and $Shld2^{-/-}$ Ig^{lo} subclones

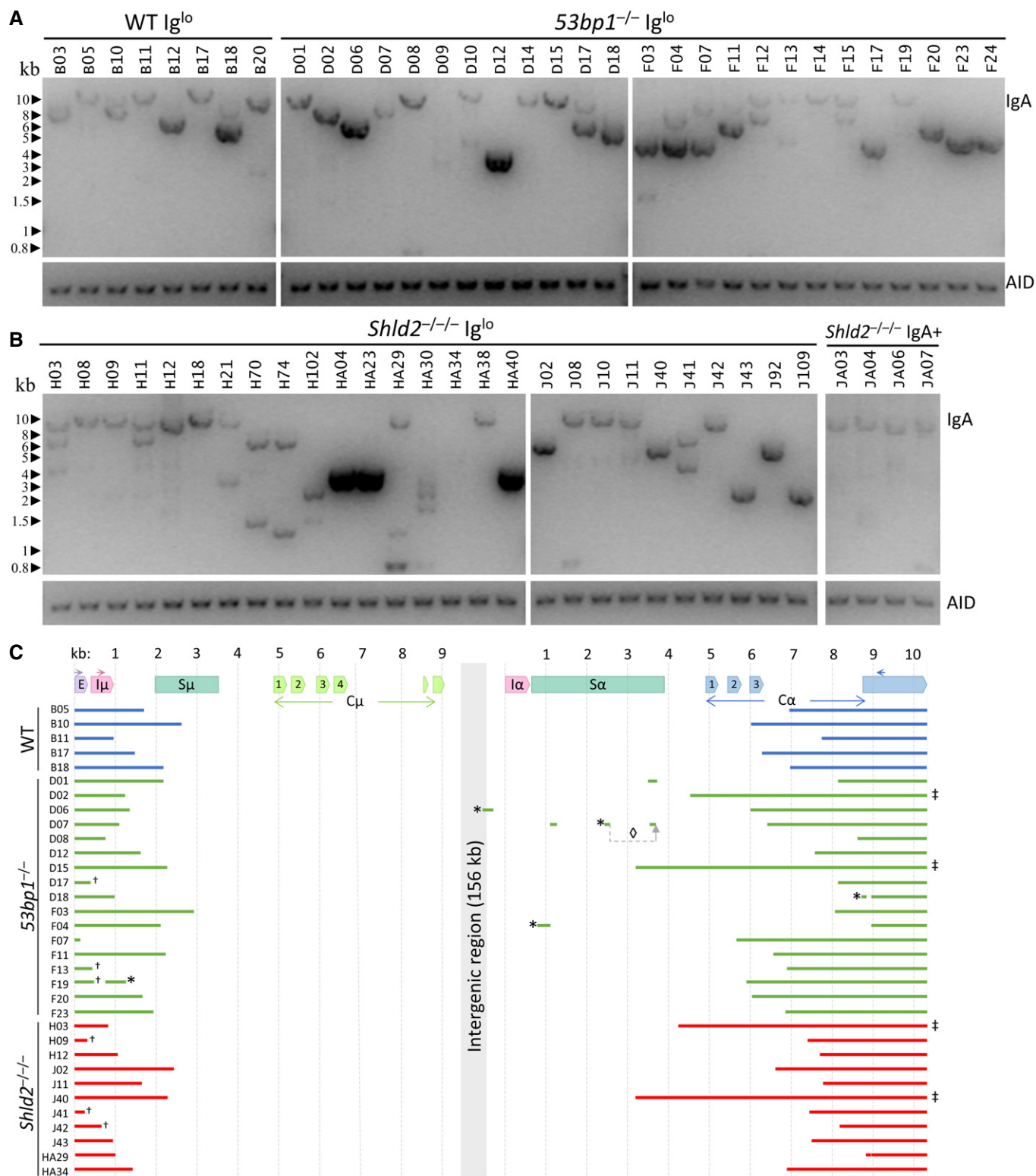


Figure 6. Loss of Ig expression in CH12 cells is accompanied by large deletions within the IgA constant region.

A Long-range PCR of Ig^{lo} subclones from WT and two independent 53bp1^{-/-} CH12 (TA and T1) clones. The Ig^{lo} subclones derived from the 53bp1^{-/-} CH12 TA clone are listed as D01-D18, while the Ig^{lo} subclones derived from the 53bp1^{-/-} CH12 T1 clone are listed as F03-F24. Gels show long-range amplicons (top) and AID genomic DNA PCR control (bottom).

B Long-range PCR as in B of Ig^{lo} subclones of two independent Shld2^{-/-} (F2 and F3) clones (left 2 panels) and IgA+ subclones from Shld2^{-/-} clone F3.

C Sequence analysis of a representative subset of long-range PCR amplicons. Symbol annotations: (*) inverted fragment, (◇) rearranged fragment order, (†) amplified with the EμF primer rather than IμF, and (‡) undamaged Cα coding sequence.

were shorter than amplicons from *Shld2*^{-/-} IgA⁺ subclones, suggesting that the Ig^{lo} amplicons had large deletions within the IgH region (Fig 6B and C). To assess the extent of these deletions, some of these long-range amplicons were sequenced (Fig 6D). Most of the sequenced amplicons had deletions of C α exons, although 12% had no deletion of coding sequence, which may be due to the capture of both productive and non-productive *Igh* alleles. Interestingly, only 6% of the *Ighm-Igha* junctions were direct joins, with the other junctions either incorporating microhomology or sequence insertion (Fig EV5), suggesting that many of these junctions are the product of alternative end joining. All together, these data show that 53BP1 and SHLD2 deficiency leads to aberrant CSR that involves loss of coding sequence in the acceptor constant region. These data thereby provide an explanation for the increased loss of Ig expression in NHEJ-deficient B-cells undergoing CSR, which supports the role of the 53BP1-Rif1-shieldin axis in inhibiting DNA resection.

Discussion

The recently characterized shieldin complex composed of SHLD1/2/3, and REV7 exhibits increased end resection during DSB repair leading to defective NHEJ and CSR. This work has been accomplished in cell lines, with the exception of REV7 (Ghezraoui *et al*, 2018). In this report, we generated *Shld2*^{-/-} mice and report that SHLD2 deficiency largely recapitulated 53BP1 deficiency (Manis *et al*, 2004) in terms of a defect in CSR and largely normal lymphocyte development and V(D)J recombination. This work establishes the shieldin complex as an essential factor in CSR *in vivo*. Furthermore, this work further shows that SHLD2 is the main effector mediating the epistatic antagonism of 53BP1 on BRCA1. The observation that *Brcal*^{A11/A11}; *Shld2*^{-/-} mice are viable with no apparent pathologies at > 27 weeks of age suggests that the loss of shieldin allows for the rescue of HR.

We observed that murine *Shld2*^{-/-} B-cells, in addition to CH12 cells deficient in 53BP1, SHLD2, and other NHEJ repair factors, exhibited an increase in an Ig^{lo} population during CSR induction. Two initial possibilities struck us as potential explanatory mechanisms: First, these cells may be temporarily decreasing Ig expression due to unrepaired DNA damage in the switch regions, a process that might be regulated by ATM (Harding *et al*, 2015). Alternatively, CSR induced an increase in non-productive recombination events (Dong *et al*, 2015) in SHLD2- and other NHEJ-deficient B-cells. Indeed, we observed that most Ig^{lo} clones from 53BP1-deficient CH12 cells were the product of non-functional CSR into the *Igha* locus, leading to the production of transcripts that were missing IgA constant region exons. These recombination events also occur in WT CH12 cells, but because the frequency of Ig^{lo} cells is reduced in these cells, the frequency of such non-productive CSR events is minimal in WT B-cells. Interestingly, the aggregate frequency IgA⁺ and Ig^{lo} populations together in WT, SHLD2-deficient, and other NHEJ-deficient B-cells is strikingly similar (Fig 3). This observation suggests that recombination at the DNA level *per se* is not necessarily reduced in 53BP1- and SHLD2-deficient cells, but a larger proportion of such recombination events are non-functional in repair-deficient cells due to excessive resectioning and loss of coding sequence. Additionally,

these non-functional recombination events may be biased toward alternative end joining as a last-ditch repair attempt (Fig EV5).

Inversional recombination has previously been observed to be increased in *53bp1*^{-/-} B-cells during CSR (Dong *et al*, 2015). Inversional recombination during CSR is predicted to lead to loss of Ig expression as constant region coding sequences downstream of variable region VDJ exon would be inverted and incapable of being translated. Curiously, however, we find that Ig^{lo} clones from 53BP1-deficient CH12 cells are largely due to loss of IgA constant region sequences during CSR and not due to inversional recombination (Fig 5). These data suggest that inversional recombination may occur at frequencies lower than previously reported (Dong *et al*, 2015). Nevertheless, we conclude that the shieldin complex promotes CSR by inhibiting excessive DNA end resection, and the presence of a significant Ig^{lo} population during CSR may be a useful proxy indicator for increased DNA resection in the *Igh* locus.

Materials and Methods

Mouse generation and husbandry

Shld2^{-/-} mice were generated by injecting Cas9 ribonucleoprotein complexes and single guide RNA(s) with spacer sequences of GTCCACTAGTCATATCACTC, TCTTTGGAAGTCCGAACGC, and TCACGATGTCCTGTCGGCTC targeting ENSMUSE00000618046 into C57Bl/6 embryos, resulting in a 251-bp del Chr14:34268371 to 34268621, as well as an insertion of GGA. These mice were backcrossed for several generations to the C57Bl/6 background. *Shld2*^{+/-} mice were bred with *Shld2*^{+/-} to generate *Shld2*^{-/-} and WT littermates for experimental use (sex-matched; ~6–8 weeks old). *53bp1*^{+/-} mice were bred with *53bp1*^{+/-} to generate *53bp1*^{-/-} and WT littermates for experimental use (sex-matched; ~8 weeks old). All mice were maintained under pathogen-free conditions. The experimental procedures were approved by the Animal Care Committee of University of Toronto. Histopathology examination carried out by Dr. S. Camilleri at the Centre for Phenogenomics (Toronto) included the following organs and tissues: calvarium, brain, eyes, ears, tongue, Harderian gland, zymbal gland, salivary glands, nasal sinuses, teeth, trachea, lungs, heart, thymus, parathyroid gland, spleen, liver, gall bladder, exocrine pancreas, endocrine pancreas, esophagus, stomach, large intestine, small intestine, urinary organs and tract, testis, epididymis, vas deference, seminal vesicle, prostate, penis, adrenal gland, lymph nodes, spinal cord, bone marrow, skeletal muscles, brown fat, and skin.

Spleen, bone marrow, thymus, and peritoneal cavity profiling

Single-cell suspensions of spleen, bone marrow, thymus, and peritoneal cavity were prepared from *Shld2*^{-/-} or WT littermate mice (6–8 weeks old). The cells were resuspended in staining buffer (PBS + 2% FBS) and incubated with mouse Fc blocker (2.4G2 mAb). As previously described (Li *et al*, 2018), splenocytes were stained with rat anti-CD45R/B220 APC (RA3-6B2; Southern Biotech; 1/150 dilution), rat anti-IgM eFluor450 (II/41; eBioscience; 1/150 dilution), rat anti-CD93 PE (AA4.1; eBioscience; 1/50 dilution), rat anti-CD23 PerCP-eFluor710 (B3B4; eBioscience; 1/100 dilution), and rat anti-

CD21/CD35 PE-Cy7 (8D9; eBioscience; 1/100 dilution); germinal center B-cells in the spleen were stained with anti-CD45R/B220 eFluor 450 (eBioscience; 1/100 dilution), GL-7 Alexa Fluor 488 (GL7; eBioscience; 1/100 dilution), and FAS/CD95 APC (15A7; eBioscience; 1/100 dilution); BM cells were stained with anti-CD45R/B220 APC, anti-IgM eFluor450, rat anti-IgD PerCP-eFluor710 (11-26c; eBioscience; 1/100 dilution), rat anti-CD43 PE-Cy7 (S7; BD Pharmingen; 1/150 dilution), rat anti-CD24 FITC (30-F1; eBioscience; 1/100 dilution), and rat anti-BP-1 PE (6C3; BioLegend; 1/33 dilution); peritoneal cells were stained with anti-CD45R/B220 APC, anti-CD23 PerCP-eFluor710, and rat anti-CD5 PE (53-7.3; eBioscience; 1/100 dilution); and thymocytes were stained with anti-CD25 FITC, anti-CD44 Super Bright 600, anti-CD4 Alexa Fluor 700, anti-CD8 α PE, anti-TCR β APC, and anti-TCR $\gamma\delta$. Stained cells were acquired on an LSR II (BD Biosciences) and analyzed by FlowJo software.

Ex vivo CSR

Splenic B-cells were purified from *Shld2*^{-/-} mice (6–8 weeks old), and age- and sex-matched littermate controls, using the EasySep Mouse B-cell Isolation Kit (Stemcell Technologies) and stimulated *in vitro* as described previously (Li et al, 2018). The stained cells were acquired on a LSR II (BD Biosciences) and analyzed by FlowJo software.

NP-specific ELISA and ELISPOT assay

Shld2^{-/-} or WT littermates (6–8 weeks old) and *53bp1*^{-/-} mice (10–12 weeks) were intraperitoneally immunized with 100 μ g of 1 mg/ml NP₂₀-CGG in PBS (Biosearch) precipitated with an equal volume of Imject Alum (Thermo) according to the manufacturer instructions. At day 21 post-immunization, sera and spleens were harvested and subjected to ELISA and ELISPOT as previously described (Li et al, 2018).

In vitro RAG1/2 and Cas9 induced switching

2×10^5 puromycin-resistant A70.2 INV-4 cells transduced with lentiCRISPRv2 (Addgene #52961) were stimulated as previously described for 4 days (Bredemeyer et al, 2006). *Aid*^{-/-} CH12 cells were electroporated with sgRNA/Cas9 vectors targeting upstream of S μ and S α as previously described (Ling et al, 2018).

Cell culture and CRISPR/Cas9 editing

Gene targeting and CH12 cells were performed as described previously (Ramachandran et al, 2016). The CH12 parental clone I (referred to above as WT CH12) was used to delete the following genes using CRISPR: *Lig4*, *Xlf*, *Ku70*, *Ku80*, *XRCC4*, and *Paxx* using sgRNA sequences listed in Table EV2. Verification of gene targeting was accomplished by sequencing. The 53BP1-, SHLD1-, SHLD2-, and SHLD3-deficient CH12 clones were previously generated (Noordermeer et al, 2018).

PCR and qPCR

RNA was isolated with TRIzol (Thermo Fisher) and cDNA was synthesized with Maxima H Minus reverse transcriptase (Thermo

Fisher) according to the manufacturer's instructions. Genomic DNA was isolated by proteinase K digest and phenol–chloroform extraction. Quantitative PCR was performed with qPCRBIOSyGreen Blue Mix (PCR Biosystems) and CFX384 Real-Time PCR Detection System (Bio-Rad) according to the manufacturers' instructions. Reverse-transcription PCR of IgM and IgA cDNA performed with Ighv_F and either IgM_R or IgA_R. Long-range PCR of the *Ighm-Igha* amplicon was accomplished using Platinum SuperFi II polymerase (Invitrogen) using the manufacturer's instructions and an 8 min polymerase extension step, using either E μ F or I μ F and C α R primers. The primers used for all reactions are listed in Table EV1.

Statistics

All analyses were performed on GraphPad Prism. For Student's *t*-tests, and two-way analysis of variance (ANOVA), *P* values of 0.05 or less were considered significant: **P* < 0.05, ***P* < 0.01, ****P* < 0.001, and *****P* < 0.0001. All error bars represent standard deviations.

Expanded View for this article is available online.

Acknowledgements

We would like to thank the Martin and Durocher laboratories for helpful discussions, and Marc Shulman for providing feedback on the manuscript. The authors would like to acknowledge Dr. S. Camilleri and the Pathology Core at The Centre for Phenogenomics for their technical services as well as Lauryl Nutter at The Centre for Phenogenomics for generation of the *Shld2*^{-/-} mutant mouse. We thank Kefei Yu for AID, LIG4, and KU80-mutant CH12 cells. This research is supported by grants from the Canadian Institutes of Health Research to D.D. (FDN143343) and to A.M. (Grant PJT-153307).

Author contributions

AKL, DD, and AM conceived the study. AKL and AM wrote the manuscript. AKL, MM, NC, CL, MB, and BW performed all of the experiments under the supervision of DD and AM.

Conflict of interest

The authors declare that they have no conflict of interest.

References

- Bothmer A, Robbiani DF, Feldhahn N, Gazumyan A, Nussenzweig A, Nussenzweig MC (2010) 53BP1 regulates DNA resection and the choice between classical and alternative end joining during class switch recombination. *J Exp Med* 207: 855–865
- Bouwman P, Aly A, Escandell JM, Pieterse M, Bartkova J, van der Gulden H, Hiddingh S, Thanasoula M, Kulkarni A, Yang Q et al (2010) 53BP1 loss rescues BRCA1 deficiency and is associated with triple-negative and BRCA-mutated breast cancers. *Nat Struct Mol Biol* 17: 688–695
- Bransteitter R, Pham P, Scharff MD, Goodman MF (2003) Activation-induced cytidine deaminase deaminates deoxycytidine on single-stranded DNA but requires the action of RNase. *Proc Natl Acad Sci USA* 100: 4102–4107
- Bredemeyer AL, Sharma GG, Huang CY, Helmink BA, Walker LM, Khor KC, Nuskey B, Sullivan KE, Pandita TK, Bassing CH et al (2006) ATM stabilizes DNA double-strand-break complexes during V(D)J recombination. *Nature* 442: 466–470

- Brinkman EK, Chen T, Amendola M, van Steensel B (2014) Easy quantitative assessment of genome editing by sequence trace decomposition. *Nucleic Acids Res* 42: e168
- Bunting SF, Callen E, Wong N, Chen HT, Polato F, Gunn A, Bothmer A, Feldhahn N, Fernandez-Capetillo O, Cao L et al (2010) 53BP1 inhibits homologous recombination in Brca1-deficient cells by blocking resection of DNA breaks. *Cell* 141: 243–254
- Callen E, Zong D, Wu W, Wong N, Stanlie A, Ishikawa M, Pavani R, Dumitrache LC, Byrum AK, Mendez-Dorantes C et al (2019) 53BP1 enforces distinct pre- and post-resection blocks on homologous recombination. *Mol Cell* 77: 26–38.e7
- Cao L, Xu X, Bunting SF, Liu J, Wang RH, Cao LL, Wu JJ, Peng TN, Chen J, Nussenzweig A et al (2009) A selective requirement for 53BP1 in the biological response to genomic instability induced by Brca1 deficiency. *Mol Cell* 35: 534–541
- Cascalho M, Wong J, Steinberg C, Wabl M (1998) Mismatch repair co-opted by hypermutation. *Science* 279: 1207–1210
- Chapman JR, Barral P, Vannier JB, Borel V, Steger M, Tomas-Loba A, Sartori AA, Adams IR, Batista FD, Boulton SJ (2013) RIF1 is essential for 53BP1-dependent nonhomologous end joining and suppression of DNA double-strand break resection. *Mol Cell* 49: 858–871
- Dev H, Chiang TW, Lescale C, de Krijger I, Martin AG, Pilger D, Coates J, Sczaniecka-Clift M, Wei W, Ostermaier M et al (2018) Shieldin complex promotes DNA end-joining and counters homologous recombination in BRCA1-null cells. *Nat Cell Biol* 20: 954–965
- Di Noia J, Neuberger MS (2002) Altering the pathway of immunoglobulin hypermutation by inhibiting uracil-DNA glycosylase. *Nature* 419: 43–48
- Di Virgilio M, Callen E, Yamane A, Zhang W, Jankovic M, Gitlin AD, Feldhahn N, Resch W, Oliveira TY, Chait BT et al (2013) Rif1 prevents resection of DNA breaks and promotes immunoglobulin class switching. *Science* 339: 711–715
- Dong J, Panchakshari RA, Zhang T, Zhang Y, Hu J, Volpi SA, Meyers RM, Ho YJ, Du Z, Robbiani DF et al (2015) Orientation-specific joining of AID-initiated DNA breaks promotes antibody class switching. *Nature* 525: 134–139
- Escribano-Diaz C, Orthwein A, Fradet-Turcotte A, Xing M, Young JT, Tkac J, Cook MA, Rosebrock AP, Munro M, Canny MD et al (2013) A cell cycle-dependent regulatory circuit composed of 53BP1-RIF1 and BRCA1-CtIP controls DNA repair pathway choice. *Mol Cell* 49: 872–883
- Findlay S, Heath J, Luo VM, Malina A, Morin T, Coulombe Y, Djerir B, Li Z, Samiei A, Simo-Cheyoy E et al (2018) SHLD2/FAM35A co-operates with REV7 to coordinate DNA double-strand break repair pathway choice. *EMBO J* 37:e100158
- Ghezraoui H, Oliveira C, Becker JR, Bilham K, Moralli D, Anzilotti C, Fischer R, Deobagkar-Lele M, Sanchiz-Calvo M, Fueyo-Marcos E et al (2018) 53BP1 cooperation with the REV7-shieldin complex underpins DNA structure-specific NHEJ. *Nature* 560: 122–127
- Gupta R, Somyajit K, Narita T, Maskey E, Stanlie A, Kremer M, Typas D, Lammers M, Mailand N, Nussenzweig A et al (2018) DNA repair network analysis reveals shieldin as a key regulator of NHEJ and PARP inhibitor sensitivity. *Cell* 173: 972–988.e923
- Harding SM, Boiarsky JA, Greenberg RA (2015) ATM dependent silencing links nucleolar chromatin reorganization to DNA damage recognition. *Cell Rep* 13: 251–259
- Hardy RR, Carmack CE, Shinton SA, Kemp JD, Hayakawa K (1991) Resolution and characterization of pro-B and pre-pro-B cell stages in normal mouse bone marrow. *J Exp Med* 173: 1213–1225
- Kenter AL (2005) Class switch recombination: an emerging mechanism. *Curr Top Microbiol Immunol* 290: 171–199
- Li C, Irrazabal T, So CC, Berru M, Du L, Lam E, Ling AK, Gommerman JL, Pan-Hammarstrom Q, Martin A (2018) The H2B deubiquitinase Usp22 promotes antibody class switch recombination by facilitating non-homologous end joining. *Nat Commun* 9: 1006
- Ling AK, So CC, Le MX, Chen AY, Hung L, Martin A (2018) Double-stranded DNA break polarity skews repair pathway choice during intrachromosomal and interchromosomal recombination. *Proc Natl Acad Sci USA* 115: 2800–2805
- Manis JP, Morales JC, Xia Z, Kutok JL, Alt FW, Carpenter PB (2004) 53BP1 links DNA damage-response pathways to immunoglobulin heavy chain class-switch recombination. *Nat Immunol* 5: 481–487
- Martin A, Bardwell PD, Woo CJ, Fan M, Shulman MJ, Scharff MD (2002) Activation-induced cytidine deaminase turns on somatic hypermutation in hybridomas. *Nature* 415: 802–806
- Martin A, Li Z, Lin DP, Bardwell PD, Iglesias-Ussel MD, Edelmann W, Scharff MD (2003) Msh2 ATPase activity is essential for somatic hypermutation at a-T basepairs and for efficient class switch recombination. *J Exp Med* 198: 1171–1178
- Masani S, Han L, Meek K, Yu K (2016) Redundant function of DNA ligase 1 and 3 in alternative end-joining during immunoglobulin class switch recombination. *Proc Natl Acad Sci USA* 113: 1261–1266
- Muramatsu M, Kinoshita K, Fagarasan S, Yamada S, Shinkai Y, Honjo T (2000) Class switch recombination and hypermutation require activation-induced cytidine deaminase (AID), a potential RNA editing enzyme. *Cell* 102: 553–563
- Noordermeer SM, Adam S, Setiawati D, Barazas M, Pettitt SJ, Ling AK, Olivieri M, Alvarez-Quilon A, Moatti N, Zimmermann M et al (2018) The shieldin complex mediates 53BP1-dependent DNA repair. *Nature* 560: 117–121
- Pan Q, Petit-Frere C, Lahdesmaki A, Gregorek H, Chrzanoska KH, Hammarstrom L (2002) Alternative end joining during switch recombination in patients with ataxia-telangiectasia. *Eur J Immunol* 32: 1300–1308
- Petersen-Mahrt SK, Harris RS, Neuberger MS (2002) AID mutates *E. coli* suggesting a DNA deamination mechanism for antibody diversification. *Nature* 418: 99–103
- Rada C, Di Noia JM, Neuberger MS (2004) Mismatch recognition and uracil excision provide complementary paths to both Ig switching and the A/T-focused phase of somatic mutation. *Mol Cell* 16: 163–171
- Ramachandran S, Haddad D, Li C, Le MX, Ling AK, So CC, Nepal RM, Gommerman JL, Yu K, Ketela T et al (2016) The SAGA deubiquitination module promotes DNA repair and class switch recombination through ATM and DNAPK-Mediated gammaH2AX formation. *Cell Rep* 15: 1554–1565
- Setiawati D, Durocher D (2019) Shieldin - the protector of DNA ends. *EMBO Rep* 20: e47560
- Tomida J, Takata KI, Bhetawal S, Person MD, Chao HP, Tang DG, Wood RD (2018) FAM35A associates with REV7 and modulates DNA damage responses of normal and BRCA1-defective cells. *EMBO J* 37: e99543
- Wiesendanger M, Kneitz B, Edelmann W, Scharff MD (2000) Somatic hypermutation in MutS homologue (MSH)3-, MSH6-, and MSH3/MSH6-deficient mice reveals a role for the MSH2-MSH6 heterodimer in modulating the base substitution pattern. *J Exp Med* 191: 579–584
- Wilson TM, Vaisman A, Martomo SA, Sullivan P, Lan L, Hanaoka F, Yasui A, Woodgate R, Gearhart PJ (2005) MSH2-MSH6 stimulates DNA polymerase eta, suggesting a role for A: T mutations in antibody genes. *J Exp Med* 201: 637–645

Xu X, Qiao W, Linke SP, Cao L, Li WM, Furth PA, Harris CC, Deng CX (2001)
Genetic interactions between tumor suppressors Brca1 and p53 in
apoptosis, cell cycle and tumorigenesis. *Nat Genet* 28: 266–271

Zimmermann M, Lotterberger F, Buonomo SB, Sfeir A, de Lange T (2013)
53BP1 regulates DSB repair using Rif1 to control 5' end resection. *Science*
339: 700–704